

# Volume, Heat, and Salt Transports through the Soya Strait and Their Seasonal and Interannual Variations

KAY I. OHSHIMA

*Institute of Low Temperature Science, Hokkaido University, Sapporo, Japan*

DAISUKE SIMIZU

*National Institute of Polar Research, Tachikawa, Japan*

NAOTO EBUCHI

*Institute of Low Temperature Science, Hokkaido University, Sapporo, Japan*

SHUTA MORISHIMA

*Ship and Offshore Structure Company, Kawasaki Heavy Industries, Ltd., Kobe, Japan*

HARUHIKO KASHIWASE

*Institute of Low Temperature Science, Hokkaido University, Sapporo, Japan*

(Manuscript received 9 September 2016, in final form 1 March 2017)

## ABSTRACT

Volume, heat, and salt transports through the Soya Strait are estimated based on measurements from high-frequency ocean radars during 2003–15 and all available hydrographic data. The baroclinic velocity structure derived from the climatological geopotential anomaly is combined with the sea surface gradient obtained from radar-derived surface velocities to estimate the absolute velocity structure. The annual-mean volume, heat, and salt transports are 0.91 Sv ( $1 \text{ Sv} \equiv 10^6 \text{ m}^3 \text{ s}^{-1}$ ), 25.5 TW, and  $31.15 \times 10^6 \text{ kg s}^{-1}$ , respectively. The volume transport exhibits strong seasonal variations, with a maximum of 1.41 Sv in August and a minimum of 0.23 Sv in January. The seasonal amplitude and phase roughly correspond to those of the Tsushima–Korea Strait. Time series of the monthly transport is presented for the 12 yr, assuming that the baroclinic components are the monthly climatological values. In cold seasons (November to April), the monthly volume transport is strongly correlated with the sea level difference between the Japan and Okhotsk Seas, and an empirical formula to estimate the transport from the sea level difference is introduced. It is likely that the sea level setup by the wind stress along the east coast of Sakhalin determines the sea level difference, which explains the seasonal and interannual wintertime variations of transport through the strait. The annual flux of water through the Soya Strait with a density greater than  $26.8\sigma_\theta$ , a potential source of Okhotsk Sea Intermediate Waters, is estimated to be 0.18 Sv.

## 1. Introduction

A part of Kuroshio enters the Japan Sea through the Tsushima–Korea Strait as the Tsushima Warm Current (TSC) and flows out through the Tsugaru Strait as the Tsugaru Warm Current (TGC) and out through the Soya/LaPerouse Strait as the Soya Warm Current

(SWC), constituting the Japan Sea Throughflow (Fig. 1). The SWC flows from the Japan Sea into the Sea of Okhotsk through the shallow Soya/LaPerouse Strait (referred to as the Soya Strait hereinafter). The Japan Sea Throughflow, including the SWC, is considered to be driven by the sea level difference between the inflow and outflow ports (Minato and Kimura 1980; Toba et al. 1982; Ohshima 1994; Lyu and Kim 2005).

Over the past decades, many investigations have estimated the transport through the Tsushima–Korea

---

Corresponding author e-mail: K. I. Ohshima, ohshima@lowtem.hokudai.ac.jp

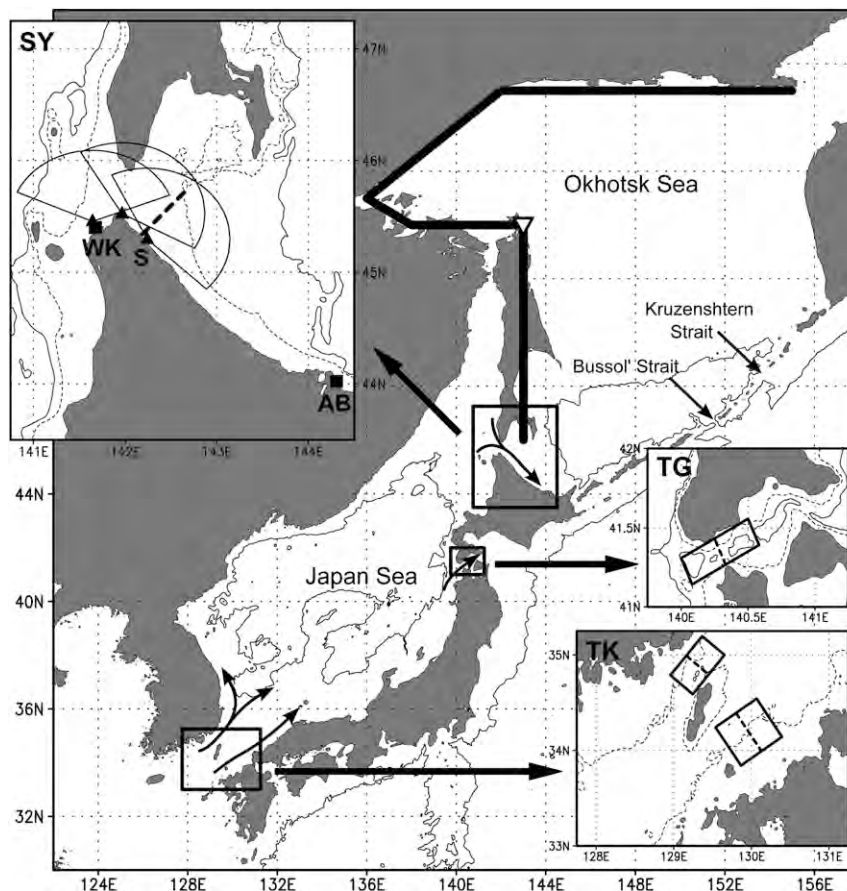


FIG. 1. A bathymetric map of the straits of the Japan Sea. Bottom contours are 2000 m in the larger map, and 100 m (dotted lines) and 200 m in the inset maps. SY, TG, and TK represent the Soya, Tsugaru, and Tsushima–Korea Straits, respectively. In the inset map of the Soya Strait, the sites of three ocean radar stations are indicated by triangles with the fan-shaped coverages of the radars. The dashed line north of the Sarufutsu radar station (S) is the section where the monthly average profile of the alongshore velocity is estimated from HF radar data. This line is used to estimate the transport. The locations of the tide gauge stations at Wakkanai (WK) and Abashiri (AB) are shown by squares. The thick solid lines along the Okhotsk coast indicate the integration route of the wind stress for the calculation of the ATW transport from Eq. (4), where the entire path and the shorter path starting from the inverted triangle are used.

Strait, mainly with acoustic Doppler current profiler (ADCP) measurements (Isobe et al. 1994, 2002; Ostrovskii et al. 2009; Teague et al. 2002, 2005; Takikawa et al. 2005; Jacobs et al. 2001; Na et al. 2009; Fukudome et al. 2010). According to these investigations, the annually averaged volume transport through the Tsushima–Korea Strait lies in the range 2.4–2.7 Sv ( $1 \text{ Sv} \equiv 10^6 \text{ m}^3 \text{ s}^{-1}$ ). There are distinct seasonal variations, with a maximum in October and a minimum in January; the amplitude of the seasonality is 1.1–1.8 Sv. On the other hand, the annually averaged volume transport through the Tsugaru Strait is suggested to lie in the range 1.4–1.5 Sv, with small seasonal amplitude of  $\sim 0.3$  Sv, according to the ADCP measurements that

have been carried out since the 1990s (Shikama 1994; Ito et al. 2003; Nishida et al. 2003).

Compared to the Tsushima–Korea and Tsugaru Straits, the flow field around the Soya Strait had been much less observed before 2000 because of logistical problems due to heavy fishing activities, the national border, and the presence of sea ice in winter. Tanaka and Nakata (1999) carried out snapshot observations of the current in the Soya Strait using shipboard ADCP. Matsuyama et al. (2006) conducted snapshot ADCP observations of the SWC off the Hokkaido coast and estimated the SWC transport to be 1.2–1.3 Sv in August 1998 and 1.5 Sv in July 2000. Long-term mooring observations at one location with a current meter (Aota

and Matsuyama 1987; Matsuyama et al. 1999) and with a bottom-mounted ADCP (Fukamachi et al. 2008, 2010) showed that the SWC becomes strong in summer and weak in winter. Fukamachi et al. (2008, 2010) also revealed a prominent seasonal variability in the vertical flow structure, with positive shear (the velocity increases toward the surface) in summer and fall and negative shear in winter and spring.

Since August 2003, the surface flow field around the Soya Strait has been continuously monitored by three high-frequency ocean radars (referred to as HF radars hereinafter; Fig. 1). Based on these radar data, Ebuchi et al. (2006, 2009) revealed the detailed surface flow structure of the SWC and its seasonal variations. Using the vertical flow structure obtained with a bottom-mounted ADCP and the surface flow field obtained with HF radars during 2004–05, Fukamachi et al. (2008) estimated the annual-mean transport of the SWC to be in the range 0.94–1.04 Sv, with a minimum in winter and a maximum in fall. In a similar way, Fukamachi et al. (2010) estimated an annual-mean transport through the Soya Strait to be 0.8–0.9 Sv, with similar seasonal variations for nearly 2 yr during 2006–08. These estimates were based on surface currents and the vertical structure of the currents at one point; the baroclinic component was therefore not evaluated appropriately. These 3-yr observations have been the only quantitative estimations of the transport. Until now, the climatological mean and the interannual variations of the transport through the Soya Strait (referred to as the SWC transport) have not been well characterized.

The primary purpose of this study is to provide climatological values of the mean and seasonal variations of the SWC transport for the first time, which has been the missing link of the Japan Sea Throughflow system. The estimation of the volume transport is based on HF radar data accumulated for 12 yr and climatological hydrography, with taking account of the baroclinic flow structure. Second, we examine the interannual variability of the SWC transport and its relationship with the sea level difference (SLD) between the Japan and Okhotsk Seas, which is considered as the driving force of the SWC. As will be shown, the transport is significantly correlated with the SLD for winter seasons but not for summer seasons. Thus, we introduce an empirical formula to estimate the volume transport from the SLD for winter seasons. Furthermore, we discuss the mechanism responsible for the seasonal and interannual variations of the volume transport and its relationship to the wind stress along the Okhotsk coast, which can be a key for understanding of the driving mechanism of the Japan Sea Throughflow. With respect to the seasonal variations of the Japan Sea Throughflow, Tsujino et al. (2008)

and Kida et al. (2016), based on numerical and analytical models, pointed out the importance of wind stress along the Okhotsk coast; this wind stress drives the changes of the SWC transport and thereby further affects changes of the transport through the Tsushima–Korea Strait.

Heat and salt/freshwater fluxes through the Soya Strait are inevitable components on the heat and salt budgets both for the Japan and Okhotsk Seas. However, these fluxes have never been estimated based on observational data. The fluxes through the Tsushima–Korea Strait have been estimated in several studies (Isobe et al. 2002; Morimoto et al. 2012). Hirose et al. (1996) examined the heat budget in the Japan Sea, considering the heat transport through the three straits. In that study, the volume transport through the Soya Strait is treated as an unknown variable, assuming a constant value with no seasonal variation. The seasonal variation of volume and heat transports through the three straits has not been adequately taken into account on the heat budget in the previous observational studies. Seo et al. (2014) evaluated the heat transports through the three straits incorporating the seasonal variations based on the high-resolution reanalysis. Regarding the Okhotsk Sea, no investigation has been made of the heat and salt budgets that incorporate the fluxes through the Soya Strait. In this study, we also attempt to evaluate the contribution of heat and salt transport through the Soya Strait on the heat and salt budgets in the Japan and Okhotsk Seas.

The SWC water also plays an important role in ventilation and water mass formation in the Okhotsk Sea. The SWC water, originating from the Kuroshio, becomes denser in winter and spring due to its high salinity. This dense SWC water can be a source of Okhotsk Sea Intermediate Water (OSIW) and further North Pacific Intermediate Water (Watanabe and Wakatsuchi 1998), in addition to the dense shelf water formed in the northwestern shelf due to high sea ice production (Shcherbina et al. 2003). We also evaluate the influx of dense SWC water that can contribute to OSIW, based on the flux dataset created in this study.

## 2. Data and processing

### a. Hydrographic data

The historical hydrographic data used in this study were obtained mainly from the Japan Oceanographic Data Center (JODC) and World Ocean Database 2005 (WOD05). Data collection in the winter has been extremely limited in the SWC region because of ice cover. To obtain information on winter hydrography, Hokkaido University carried out hydrographic observations with

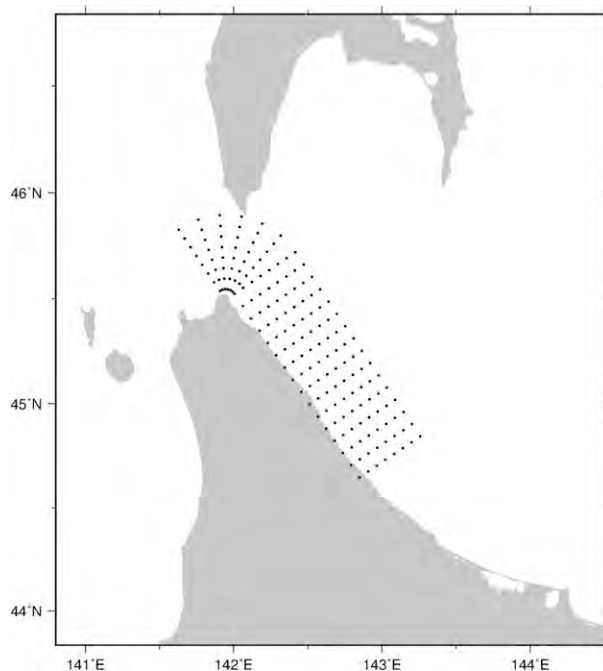


FIG. 2. Coordinate system and grid points used for vertical section dataset.

the icebreaker *Soya* in January and February from 1996 to 1999 with the cooperation of the Japan Coast Guard (Mizuta et al. 2004). Further, we have conducted conductivity–temperature–depth (CTD) tag observations by using instrumented sea lions and seals during 2011–14. The addition of these data covered the data-void months of January–March and the area around the national border near the strait. These additions enabled us to create a dataset that covered the full annual cycle. We also added observational data taken by the Hokkaido Fisheries Agency and the Japan Coast Guard, which have not yet been incorporated into the JODC and WOD05 digital archives.

We used only data that include both temperature and salinity components. Datasets were created for seven standard depths (0, 10, 20, 30, 50, 75, and 100 m). Taking advantage of the alongshore uniformity of the temperature, salinity, velocity, and bottom contours (Itoh and Ohshima 2000; Odamaki 1994), we constructed a two-dimensional dataset for the cross-shore section of the SWC. We used the station data in the upstream region of the SWC, including the Soya Strait area where there were radar data (gridded dots in Fig. 2).

Before the construction of the two-dimensional dataset, we carried out a quality-control check of the data. First, we chose a coordinate system parallel with the coast, except in the area around the Soya Strait, where we adopted a rotated coordinate system to

facilitate characterization of the turning of the current (Fig. 2). At all the grid points designated in Fig. 2, we calculated the mean and standard deviation of the potential temperature and salinity of all the stations within a distance of 4 km in the cross-shore direction and a distance of 12 km in the alongshore direction. Data that fell outside three standard deviations from the mean at each depth were eliminated. Based on this quality-control procedure, 3.1% of the original station data were removed. Figure 3 shows the positions of all of the quality-controlled stations for temperature and salinity data for each month. The quality-controlled data contains 3362 stations in total.

A cross-shore section dataset with 5.5-km bins was then constructed based on all the quality-controlled data. To reflect the current structure around the region off Sarufutsu, where the radar data are used as combination data, a Gaussian weighting function with an  $e$ -folding scale of 60 km was applied in the alongshore direction, with the center northwest of Sarufutsu. To generate monthly data, a Gaussian weighting function was also applied to the observation times, with its center at the middle of each month and an  $e$ -folding time of 20 days. We used the data within  $\pm 30$  days from the middle of each month.

#### b. HF ocean radar

The HF radar stations used in this study are located around the Soya Strait (triangles in Fig. 1). This SeaSonde HF radar system was manufactured by CODAR Ocean Sensors, Ltd. (Barrick et al. 1977; Barrick and Lipa 1997). The frequency of the radars is 13.9 MHz, and the range and azimuth resolutions are 3 km and  $5^\circ$ , respectively. The HF radar covers a range of approximately 70 km from the coast. The radar stations have been operated by the Institute of Low Temperature Science of Hokkaido University since August 2003. The Sarufutsu radar station stopped operating after August 2015 because the antenna was damaged by a severe storm. Therefore, data were continuously accumulated for 12 yr from the three radar stations.

Surface current vectors at 1-hourly intervals were calculated for grid cells with dimensions  $3 \times 3 \text{ km}^2$  from the radial velocity components observed by the radars using a least squares method (Ebuchi et al. 2006). These data were filtered with a 25-h running average, and daily and monthly averages were then calculated. Comparison of radar-derived hourly velocities with those from drifting buoys and shipboard ADCPs showed the root-mean-square difference of  $\sim 20 \text{ cm s}^{-1}$  with negligible bias (Ebuchi et al. 2006). Averaging would reduce the random errors, and thus the daily and monthly velocities would have errors of only  $\sim 4$  and  $\sim 1 \text{ cm s}^{-1}$ , respectively.

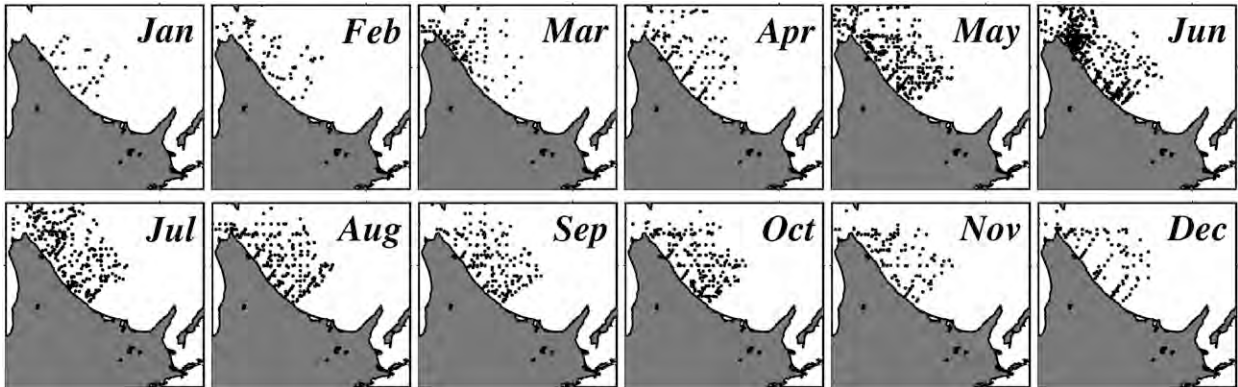


FIG. 3. Positions of all of the quality-controlled stations for temperature and salinity data for each month.

This study analyzed data obtained over a period of 12 full years, from August 2003 to August 2015. In this study, monthly averages of 12-yr data are regarded as the climatological values. We used the radar data evaluated along the line north of the Sarufutsu station (dashed line in Fig. 1). This line was chosen because it yielded high-quality data from the two radars (Ebuchi et al. 2006) and is a line representative of the vertical section dataset. The average percentage acquisition of velocity data with quality control along this line was 95% during the whole period, with a minimum rate in February of 70%. We were missing whole monthly data only for January 2015 because of the antenna problem. Data missing in February was mostly due to the presence of sea ice. We regarded a grid cell for which the data deficit exceeded 60% in a month to be a cell without data (a no-data cell) in that year. No-data cells existed only in February for 5 yr in one to four cells in offshore areas. The following method was used to interpolate data in a given year for a no-data cell. First, for the remaining data cells, the ratios of the yearly value to the climatological value were calculated and averaged for each year. Then the climatological value of the no-data cell was multiplied by this average ratio and used as that yearly data.

The velocity data obtained by the radars include a component due to wind drift; we attempted to remove this component first. Fukamachi et al. (2008), based on comparison with the ADCP data, suggested that the wind drift is directed at  $19.3^\circ$  to the right of the wind with a speed reduction factor of 1.6%. Using this angle and reduction factor, the daily wind drift components were calculated from the daily wind data and then removed from the original daily radar velocity. As the wind data, we used the daily nearby operational weather forecasting data from the mesoscale grid point values (GPV) provided by the Japan Meteorological Agency. We also used the speed reduction factor and turning

angle proposed by Zhang et al. (2016) and confirmed that the results are almost the same.

### 3. Climatological dataset

#### a. Vertical section of temperature and salinity

Figure 4 shows the vertical section of the monthly averaged temperature, salinity, and potential density. The results are consistent with those of Aota (1975), Itoh and Ohshima (2000), and Itoh et al. (2003). Warm, saline SWC water with a salinity of 33–34 occupies 20–40 km from the coast throughout the year, with a maximum extent in September. During November–February, cold freshwater with a salinity less than 32.5 is dominant from the surface to a depth of  $\sim 50$  m offshore of 20–40 km or more from the coast. This freshwater reflects the influence of the Amur River via the East Sakhalin Current and/or ice melting. During summer (June to September), the cold water belt near the surface is represented at about 30–40 km from the coast (Ishizu et al. 2008). The density map (Fig. 4c) shows that lighter, warm water from the Japan Sea is trapped by the coast in summer (clearly shown from July to October), while denser, saline water from the Japan Sea is trapped near the bottom in winter (December to March).

#### b. Calculation of geostrophic currents

To calculate the geopotential anomaly at a point shallower than the reference depth (85 m), the value of the geopotential anomaly at the bottom level ( $z = z_0$ ) is extrapolated horizontally from the next two offshore grid points: half the value of the difference between the two offshore grid points is extrapolated, as expressed in the following equation:

$$D(x, z_0) = D(x + 1, z_0) + 0.5[D(x + 1, z_0) - D(x + 2, z_0)], \quad (1)$$

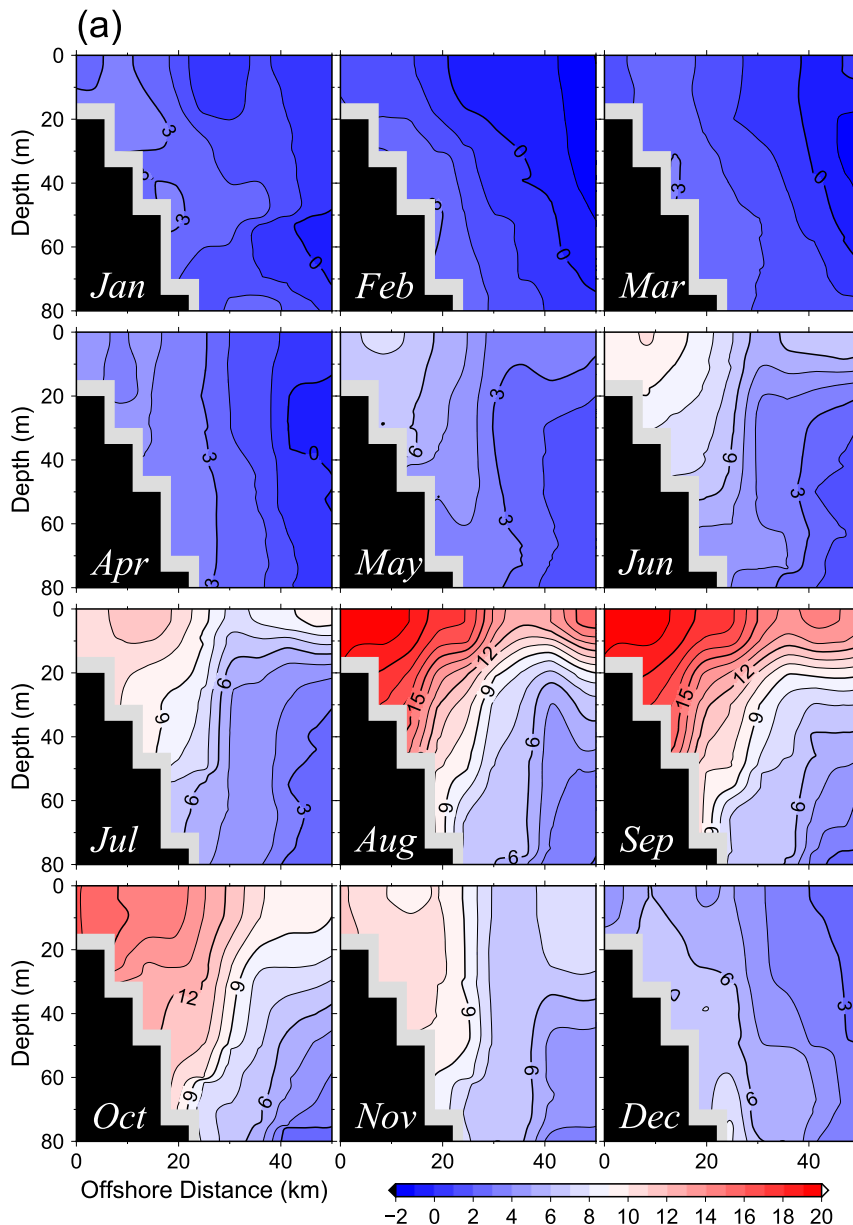


FIG. 4. Vertical section of the monthly averaged (a) temperature ( $^{\circ}\text{C}$ ), (b) salinity, and (c) potential density  $\sigma_{\theta}$ . Contour intervals are  $1^{\circ}\text{C}$ , 0.25, and  $0.25\sigma_{\theta}$  for temperature, salinity, and potential density, respectively. The section most reflects the line north of Sarufutsu (dashed line in Fig. 1).

where  $D(x, z)$  is the geopotential anomaly,  $x$  is the grid number pointing offshore, and  $z$  is the vertical grid number. We also carried out the extrapolation  $D(x, z_0) = D(x + 1, z_0)$ , in which the geostrophic current at the bottom level ( $z_0$ ) between  $x$  and  $x + 1$  is zero, and the extrapolation  $D(x, z_0) = D(x + 1, z_0) + [D(x + 1, z_0) - D(x + 2, z_0)]$ , in which the offshore  $D$  is linearly extrapolated to  $D(x, z_0)$  by using the gradient of  $D$  between the offshore nearest two grid points ( $x + 1$ ) and ( $x + 2$ ). In both cases, the relative

differences from the case of Eq. (1) in the total transport estimated in the later sections are at most  $\sim 3\%$  and thus most of our results are insensitive to the extrapolation method.

Geostrophic currents were calculated based on geopotential anomalies derived in the manner described above and are shown in Fig. 5a. Hereinafter, these velocities from the geopotential anomalies are defined to be the baroclinic components of the currents. Note that the vertical integral of the baroclinic velocity is nonzero

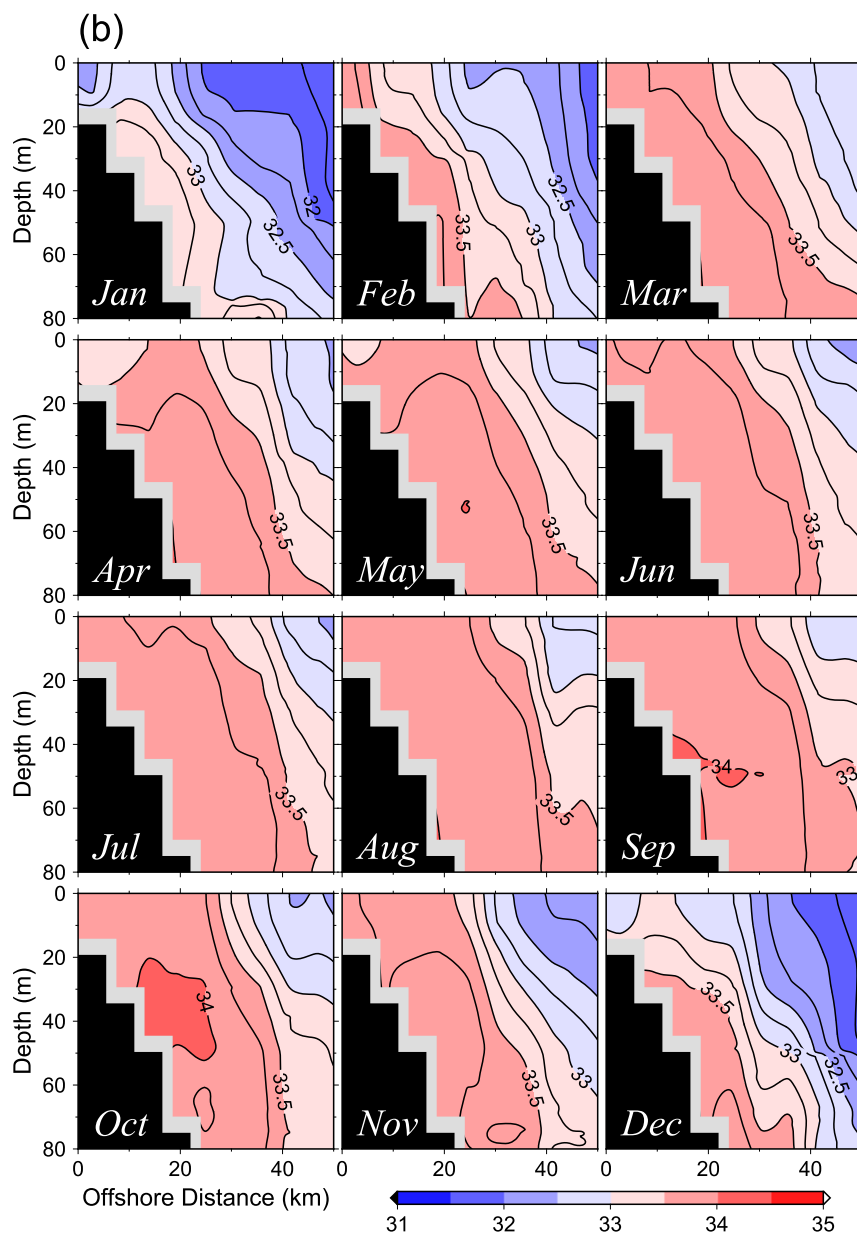


FIG. 4. (Continued)

in this definition. In summer (August–September), a strong southeastward flow appears with the core around 15–25 km from the coast and a maximum velocity of 40–50  $\text{cm s}^{-1}$ . On the other hand, the countercurrent appears around 35–40 km from the coast throughout the year. These features are consistent with the baroclinic flow structure observed with the ADCP (Matsuyama et al. 2006).

### c. Estimation of absolute velocity

The surface velocity can be obtained directly from the HF radar, and the baroclinic velocity component at the

surface was obtained in the previous section. The difference of these two velocities should be the barotropic velocity component. As the climatological surface velocity, we used the monthly radar velocity off Sarufutsu (dashed line in Fig. 1) from the 12-yr average. Once the barotropic component is given, the absolute velocity can be obtained from the sum of the barotropic and baroclinic components for the whole section.

The monthly absolute velocities are shown in Fig. 5b. In the current core, which is located about 20–30 km from the coast, the vertical shear is generally positive from July to October and is negative from November to

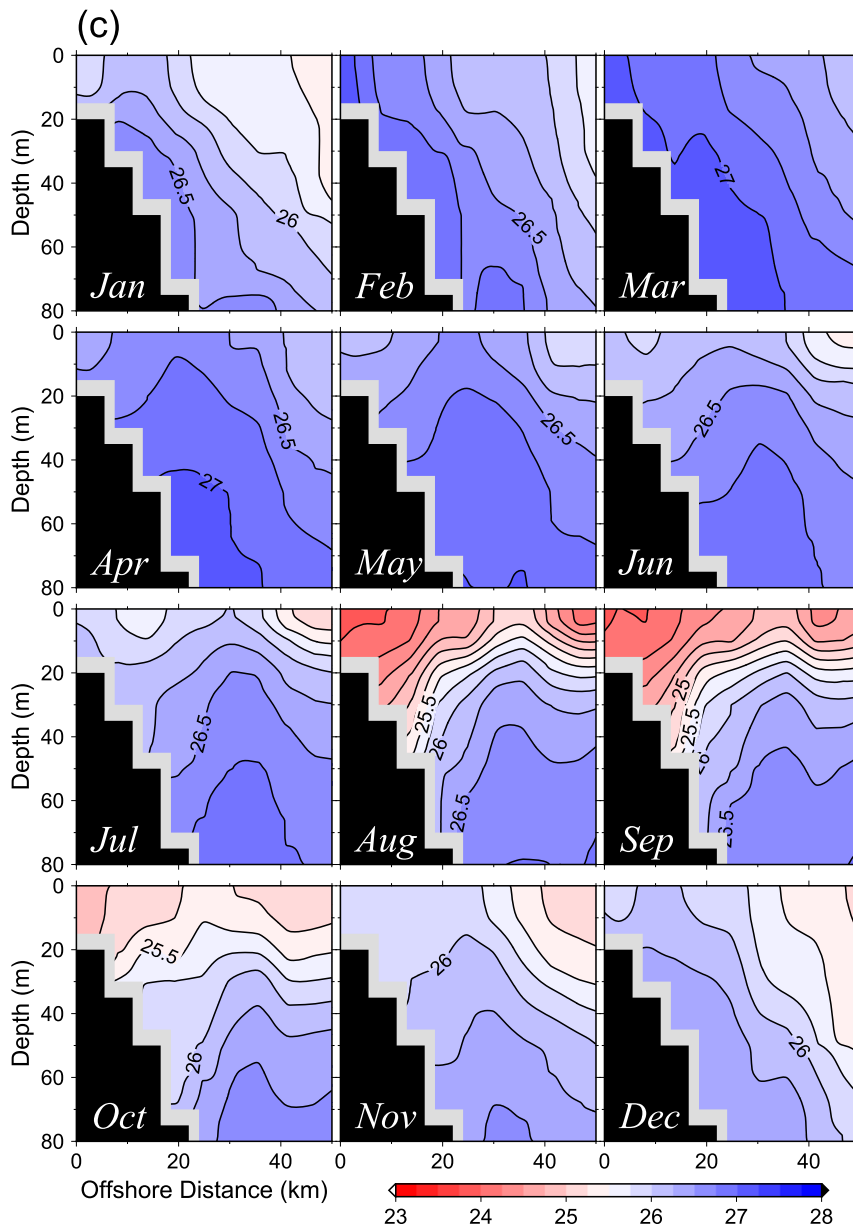


FIG. 4. (Continued)

May. This pattern is associated with the inflow of lighter (warmer) water nearshore in summer and fall and denser (saltier) water nearshore in winter and spring via the thermal wind relationship. In warm seasons, peak currents exceed  $80 \text{ cm s}^{-1}$  near the surface. These vertical structures of the velocity coincide well with the structures observed with the bottom-mounted ADCP (Fukamachi et al. 2008, 2010).

#### d. Calculation of volume transport

The volume transport  $Fv$  of the SWC was calculated as follows:

$$Fv = \iint v dA, \quad (2)$$

where  $v$  and  $A$  are the alongshore velocity and area of a section of the SWC, respectively. Specifically, the alongshore velocity was first multiplied by the corresponding cross-sectional area to calculate volume transport between adjacent grid points. The total volume transport was then calculated by integrating from the coast, where the vertically averaged velocity is assumed to be zero, to the first zero-crossing point of the surface velocity.

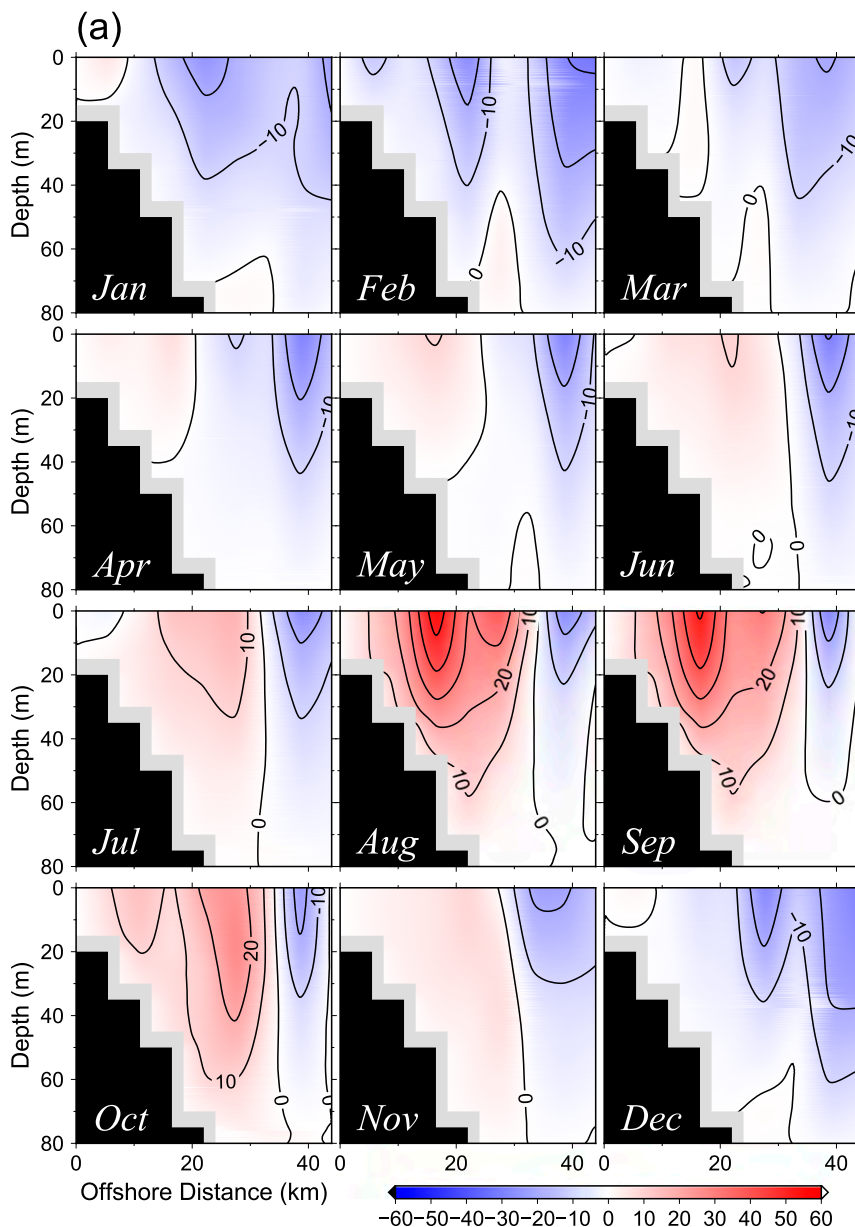


FIG. 5. Vertical sections of the monthly means of (a) baroclinic and (b) absolute (barotropic plus baroclinic components) alongshore velocities. Contour interval is  $10 \text{ cm s}^{-1}$ . Positive values indicate a southeastward current. The section most reflects the line north of Sarufutsu (dashed line in Fig. 1).

Figure 6a shows the seasonal variations of the total SWC volume transport (solid lines), its barotropic component (dashed lines), and its baroclinic component (dotted lines) derived from Fig. 5a. These monthly values are also listed in Table 1. The transport exhibits large seasonal variations, with a minimum in January and a maximum in August. The annual average of  $0.91 \text{ Sv}$  is slightly smaller (by  $\sim 10\%$ ) than the estimation during 2004–05 by Fukamachi et al. (2008), while slightly larger (by  $\sim 10\%$ ) than the estimation during 2006–08 by Fukamachi et al. (2010). As shown in

Fig. 6b, the transport (gray lines) shows seasonal variations similar to those of the sea level difference between Wakkanai and Abashiri (solid lines) and the integrated wind stress in the Okhotsk Sea (dotted lines), which will be discussed in section 6. Based on cross-section observations over the SWC, Matsuyama et al. (2006) estimated the volume transport of the SWC to be  $1.2\text{--}1.3 \text{ Sv}$  in August 1998 and  $1.5 \text{ Sv}$  in July 2000. The baroclinic component was estimated to be  $13\%\text{--}15\%$  of the total transport. These volume transports and the contributions of the baroclinic

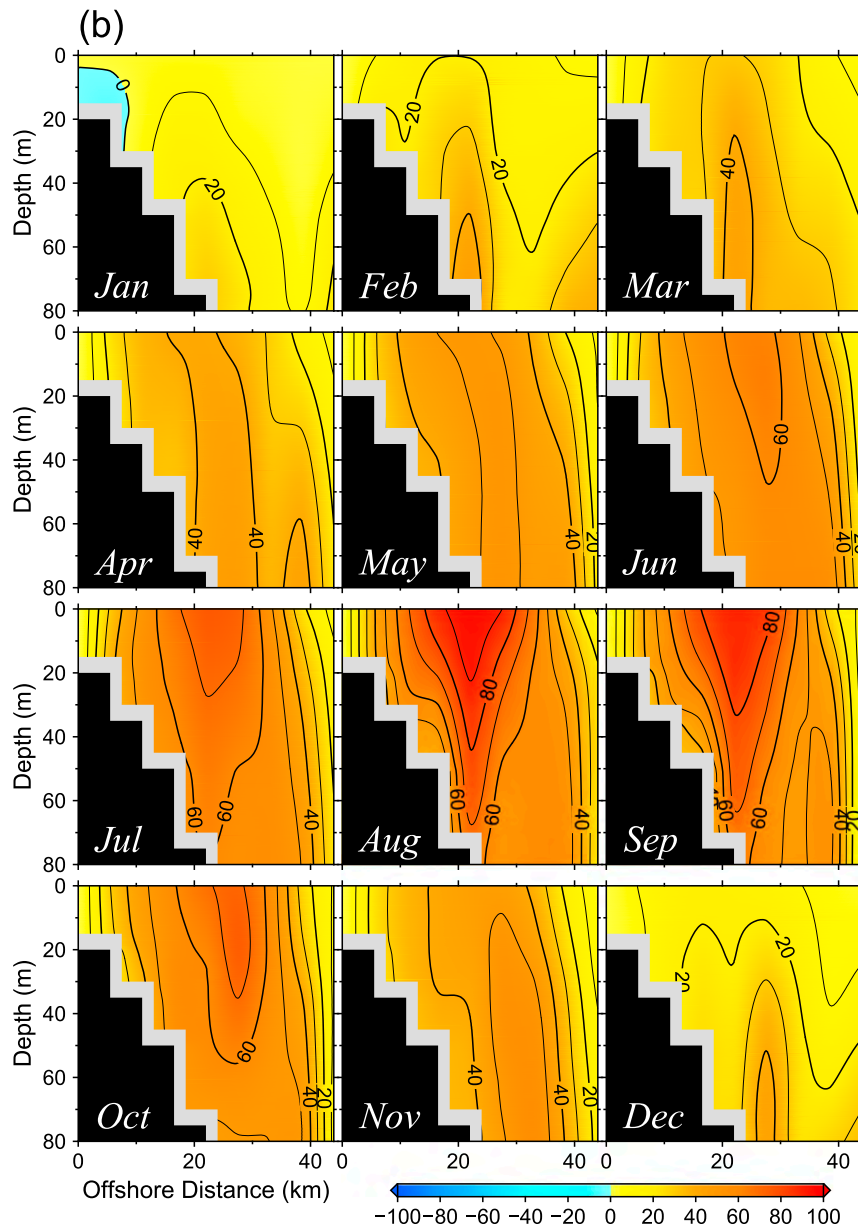


FIG. 5. (Continued)

component are roughly consistent with our climatology (Table 1).

#### 4. Interannual variability of the transport and its relationship to sea level differences

We examine the interannual variability of the SWC transport based on 12-yr data during the period of HF radar observations. We do not have enough hydrographic data to document the yearly variations of the baroclinic flow component. The baroclinic component is much smaller than the barotropic component on the transport (Fig. 6a). In this

paper, the baroclinic component for a given month of a certain year is assumed to equal the monthly climatological value listed in Table 1. In this way, the total transport of the SWC is calculated for 12 yr, and its time series is presented in Fig. 7a. The variations of the estimated transport roughly correspond to those reported by Fukamachi et al. (2008, 2010), as shown in Fig. 7b).

In previous studies (Aota and Matsuyama 1987; Ebuchi et al. 2006), the SWC velocity was found to be well correlated with the sea level difference between the two seas (specifically Wakkanai–Abashiri; see Fig. 1 for the locations) on seasonal and subinertial time scales. We thus

examine the relationship between the SWC transport and the SLD. We used the monthly data of raw sea levels and sea levels barometrically adjusted by atmospheric pressure, with 1 cm corresponding to 1 hPa. When we used the raw sea level data without a barometric correction, we obtained slightly or somewhat higher correlations than when we used barometrically corrected sea level data in almost all the analyses. This result might be due to the fact that the current across the strait by the SLD could adjust very quickly with gravity waves (Ohshima 1994; Kida et al. 2016). Hereinafter, we show the results using raw sea level data without a barometric correction. When we used barometrically corrected sea levels, we obtained basically similar results and the discussion would not have changed. We used monthly sea level and atmospheric pressure data at Wakkanai and Abashiri provided by the Coastal Movements Data Center and Japan Meteorological Agency, respectively.

Figure 8a shows scatterplots of the SLD and SWC transports; the high correlation between the two is clearly apparent. This high correlation arises largely from the similarity of their seasonal variations (Fig. 6b). To extract the anomalies from the seasonal signals, we plotted the anomalies (raw monthly data – climatological monthly data) of SLD versus SWC transport (Figs. 8b,c). It is found that the transport anomalies are strongly correlated with those of SLD from November to April (the correlation coefficient  $R$  is 0.73) but not from May to October ( $R = 0.31$ ), where  $R$  for the 99% significance level is 0.31. It is noted that one outlier of April 2013 was excluded in Fig. 8b. Good correspondence in the winter and bad correspondence in the summer were also identified between the transport from the ADCP observation and SLD (Fukamachi et al. 2008, 2010). Figure 9 shows the monthly variation of the correlation between anomalies of the SLD and SWC transport, superimposed on that of baroclinic transport, which can be a measure of vertical flow structure. Positive and negative transports correspond to surface-intensified and bottom-intensified structures, respectively. The correlation is relatively high in the months when the flow structure is bottom intensified.

If the SWC were driven by the sea level difference under the framework of inviscid fluid, the sea level at Abashiri would be equal to that at Wakkanai by the geostrophic control (Toulany and Garrett 1984). In reality, the SWC is trapped over the relatively shallow slope along the coast and dissipated mainly by the bottom friction, and a sea level drop occurs efficiently near the coast, as shown in the numerical model (Ohshima and Wakatsuchi 1990). In seasons of bottom-intensified flow, when the transport is well correlated with the SLD, the drop in sea level is likely a reflection of the dynamical balance between the pressure gradient along the flow and bottom friction. However, in seasons of

surface-intensified flow, the SLD is not necessarily determined by such balance. Another mechanism would affect the determination of the SLD. The specific mechanism is out of the scope in this study.

Based on the nearly linear relationship shown in Fig. 8b, for winter seasons (November–April) we introduce an empirical formula from which the SWC transport is inferred from the SLD on a monthly basis as follows:

$$Fv(\text{Sv}) = a[\eta(\text{cm}) - \eta_m(\text{cm})] + Fv_m(\text{Sv}), \quad (3)$$

where  $Fv$  is the SWC volume transport,  $a$  ( $=0.0418$ ) is the inclination of the regression line in Fig. 8b,  $\eta$  is the SLD in an individual month of a certain year,  $\eta_m$  is the monthly climatology of the SLD, and  $Fv_m$  is the monthly climatology of the SWC volume transport (Table 1). The volume transport estimated from the empirical equation [Eq.(3)] is shown by the thick dotted lines in Fig. 7b. It is found that the empirical formula can provide reasonable transport values.

## 5. Relationship with the transports through the Tsushima–Korea and Tsugaru Straits

Here, we discuss the SWC transport in terms of its relation to the transports through the Tsushima–Korea and Tsugaru Straits, referred to as the Tsushima Warm Current (TSC) and Tsugaru Warm Current (TGC) transports, respectively. Several observational studies have estimated the annual-mean and seasonal variations of the TSC transport. Based on results from an array of bottom-mounted ADCPs during 1999–2000, Teague et al. (2002) estimated that the annual-mean transport was 2.7 Sv, with a maximum of 3.5 Sv in October and a minimum of 1.7 Sv in January. Based on repeated shipboard ADCP observations from 1997 through 2002, Takikawa et al. (2005) showed that the annual-mean transport was 2.6 Sv, with a maximum of 3.2 Sv in October and a minimum of 1.8 Sv in January. Fukudome et al. (2010) extended their study to the period 1997–2007. Other investigations (e.g., Lyu and Kim 2003; Isobe et al. 1994, 2002; Takikawa and Yoon 2005) reported similar annual-mean values (2.4–2.7 Sv) and similar seasonal amplitudes.

The observations have been limited in the TGC compared to the TSC. Based on results from bottom-mounted ADCPs, Shikama (1994) showed that the annual-mean TGC transport is 1.4 Sv, with small seasonal variations. Based on high-resolution shipboard ADCP observations during 1999–2000, Ito et al. (2003) estimated the annual-mean transport to be 1.5 Sv. From

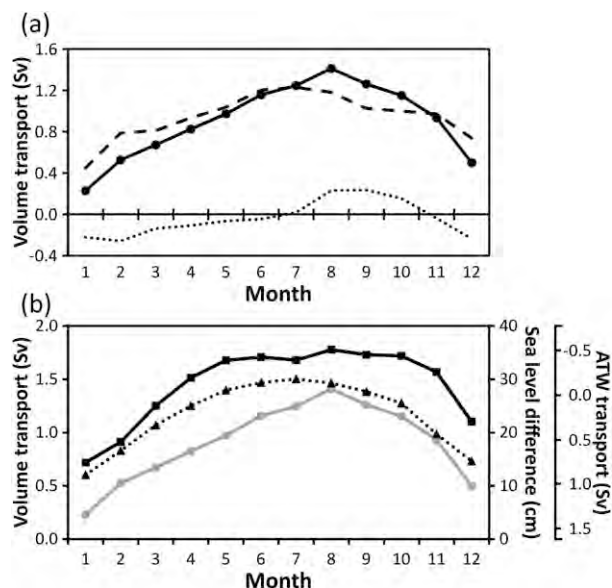


FIG. 6. Seasonal variations of the SWC volume transport, sea level difference, and ATW transport. (a) The total SWC volume transport (solid), its barotropic component (dashed), and its baroclinic component (dotted) estimated in this study. (b) Sea level difference between Wakkanai and Abashiri (solid) and the ATW transport (dotted) integrated along the route shown in Fig. 1, with the total SWC transport (gray). The scales of the sea level difference and ATW transport are indicated on the right axis and the ATW scale is inverted.

the repeated shipboard ADCP observations during 1993–99, Nishida et al. (2003) estimated the annual-mean transport to be 1.5 Sv, with small seasonal variations of  $\sim 0.3$  Sv.

In terms of annual means, the sum of the SWC transport estimated in this study (0.91 Sv) and the TGC transport (1.5 Sv) approximately coincides with the TSC

transport. Figure 10 compares the seasonal variations of the SWC transport derived from this study and TSC transport from Fukudome et al. (2010) in the climatological mean. The variations of the two transports are similar in phase and amplitude. This implies small seasonal variation in the TGC transport, which is consistent with the previous limited observations. In brief, the TSC transport is portioned to TGC by  $\sim 60\%$  and to SWC by  $\sim 40\%$  in the annual mean, and a major part of the seasonal variation in TSC transport is shared by that in SWC transport.

## 6. Mechanism of transport variation

Here, we discuss the mechanism responsible for variations of the SWC transport. Given the idea that the SWC, a part of the Japan Sea Throughflow, is driven by the SLD through the Soya Strait, we should consider the mechanism responsible for the SLD variations. This also leads to an understanding of the mechanism responsible for variations of the Japan Sea Throughflow.

On subinertial and seasonal time scales, high correlations between the SWC velocity and the SLD between the two seas have been reported in several studies (Matsuyama et al. 1999; Ebuchi et al. 2006, 2009; Fukamachi et al. 2008, 2010). On the subinertial period, Ebuchi et al. (2009) suggested that the SWC variations are caused by the SLD through the strait, which is set up by coastally trapped waves generated by the wind stress along the east coast of Sakhalin (Mizuta et al. 2004). On a seasonal time scale, the coastal branch of the East Sakhalin Current is driven in winter by the dominant northerly or northwesterly wind along the east coast of Sakhalin and farther upstream along the coast (Simizu and Ohshima 2006; Ohshima and Simizu 2008).

TABLE 1. Monthly and annual volume, heat, and salt transports through the Soya Strait estimated in this study. The error bounds in the total transports are standard deviations for the 12 yr 2003–15. For the volume transport, barotropic (column 3) and baroclinic (column 4) components are also shown. Dense water (DW) in the last column is defined as water with a potential density greater than  $26.8\sigma_\theta$ .

Month	Total (Sv)	Barotropic (Sv)	Baroclinic (Sv)	Heat flux (TW)	Salt flux ( $10^6 \text{ kg s}^{-1}$ )	DW flux (Sv)
1	$0.23 \pm 0.07$	0.45	-0.22	1.64	7.67	0.00
2	$0.53 \pm 0.13$	0.79	-0.26	1.59	17.86	0.09
3	$0.67 \pm 0.17$	0.81	-0.14	4.10	23.13	0.50
4	$0.82 \pm 0.19$	0.93	-0.11	8.49	28.34	0.50
5	$0.98 \pm 0.17$	1.05	-0.07	15.79	33.50	0.49
6	$1.16 \pm 0.25$	1.21	-0.05	25.63	39.83	0.33
7	$1.25 \pm 0.18$	1.23	0.02	35.84	42.97	0.23
8	$1.41 \pm 0.22$	1.18	0.23	63.11	48.58	0.01
9	$1.26 \pm 0.21$	1.03	0.23	60.64	43.47	0.00
10	$1.15 \pm 0.24$	1.00	0.15	49.09	39.61	0.00
11	$0.93 \pm 0.21$	0.97	-0.04	29.48	31.90	0.00
12	$0.50 \pm 0.27$	0.74	-0.24	10.79	16.91	0.00
mean	$0.91 \pm 0.07$	0.95	-0.04	25.52	31.15	0.18

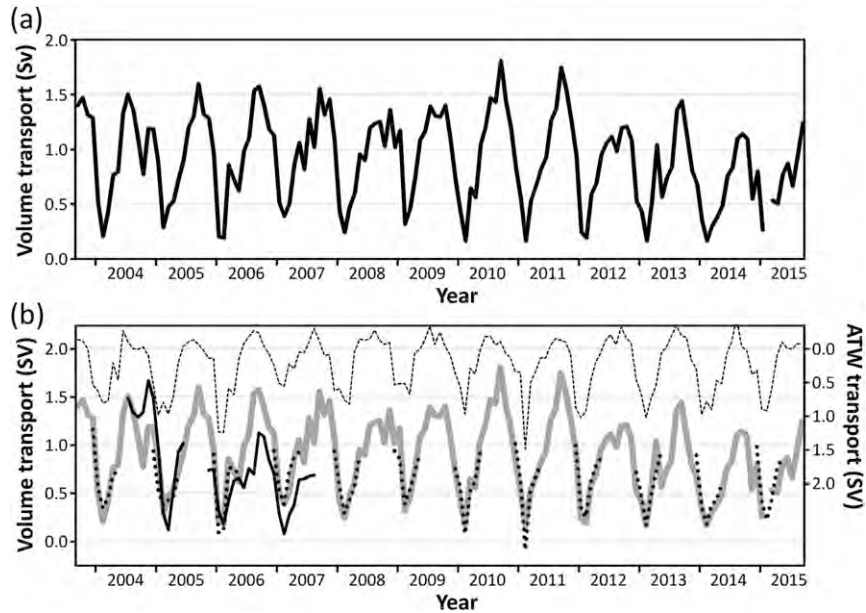


FIG. 7. Time series of monthly SWC transport and ATW transport for the 12 yr from August 2003 to August 2015. (a) The SWC transport estimated in this study. (b) The transport estimated from ADCP and HF radar by Fukamachi et al. (2008, 2010) (thin solid), the transport estimated based on the empirical equation [Eq. (3)] from the sea level difference between Wakkanai and Abashiri (thick dotted), and the ATW transport (thin dotted). The scale of the ATW transport is indicated on the right axis and inverted. In (b), the SWC volume transport estimated in this study is also superimposed (thick gray).

This alongshore wind stress also induces the setup of the sea level in winter. As a result, the sea level along the coast in the Sea of Okhotsk shows peculiar seasonal variations, with a maximum in winter and a minimum in summer, a pattern that cannot be explained by the annual cycle of atmospheric heat flux (Nakanowatari and Ohshima 2014). This variation extends to the Hokkaido coast and raises the winter sea level toward the coast on the Okhotsk side around the Soya Strait. We propose that this elevation of sea level causes a reduction of the SLD through the Soya Strait and thus a decrease of SWC transport. It should be noted that advection of low-salinity water originating from the Amur River via the East Sakhalin Current is an additional cause of winter sea level rise at the Hokkaido coast (Itoh and Ohshima 2000) but is likely of secondary importance (Nakanowatari and Ohshima 2014). As shown in Nakanowatari and Ohshima (2014), interannual variability of the winter sea level is also explained by that of the alongshore wind in the Sea of Okhotsk.

The setup of the coastal-trapped current and sea level along the east Sakhalin coast can be interpreted as arrested topographic waves (ATW), as discussed in Simizu and Ohshima (2006). According to Csanady (1978), the volume transport of ATW,  $V_{ATW}$ , is governed by the wind stress over the coast from which

coastally trapped waves (CTWs) propagate and is determined by the equation

$$V_{ATW} = \int_0^{y_1} \tau_y / (\rho_w f) dy, \quad (4)$$

where a right-handed coordinate system is used, with the positive  $x$  axis pointing to the offshore direction and the  $y$  axis lying along the coastline at  $x = 0$ ;  $\tau_y$  is the alongshore component of the wind stress;  $\rho_w$  is the density of seawater; and  $f$  is the Coriolis parameter. Equation (4) implies that the alongshore transport at  $y_1$  becomes the sum of all backward Ekman transport to or from the coast. To calculate wind stress we used a stability-independent drag coefficient following Large and Pond (1981).

We adopted the ATW transport integrated from Eq. (4) as an index of the wind forcing, with the integration path indicated by the thick solid lines in Fig. 1. We used the entire path and the shorter path starting from the inverted triangle. We obtained similar results in both cases. Hereinafter, we show the results using the shorter path because those results show slightly higher correlation for most of the analyses. For wind data we used the European Centre for Medium-Range Weather Forecasts interim reanalysis (ERA-Interim) dataset for the

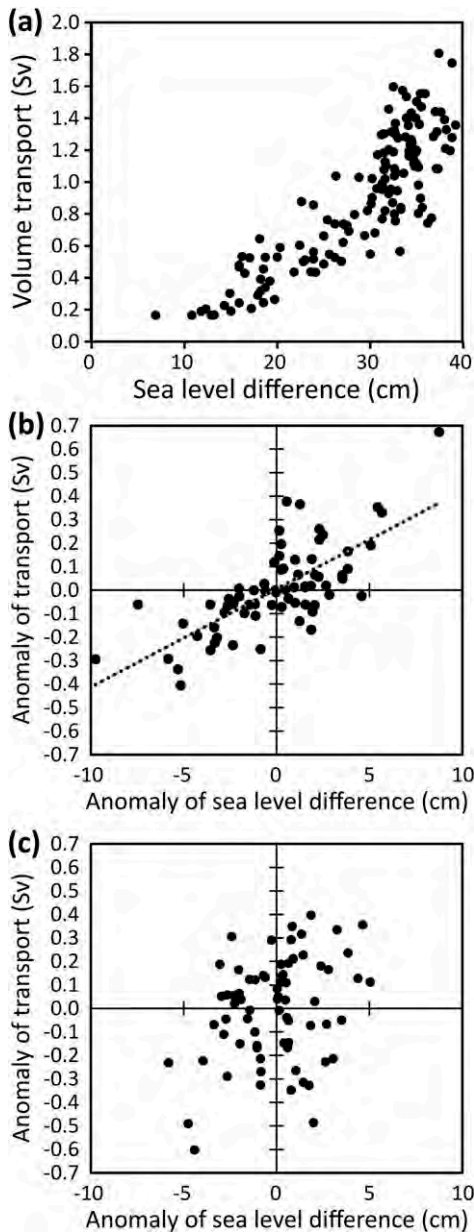


FIG. 8. Scatterplots of sea level difference between Wakkanai and Abashiri vs SWC transport on a monthly basis from (a) original raw data for all seasons, (b) anomalies from climatological monthly values for November to April, and (c) those for May to October. The dotted line in (b) is the regression line, which is used in the empirical equation [Eq. (3)] to estimate the SWC transport.

period 1979–2015, with the resolution of  $0.5^\circ \times 0.5^\circ$ . First, the daily mean wind stresses were calculated from the 6-hourly wind data at 10 m above the sea surface, and then the monthly averaged ATW transports were calculated. We also used the reanalysis data (ERA-40) with the same resolution for the period 1971–78, when ERA-Interim data are not available. To remove the bias

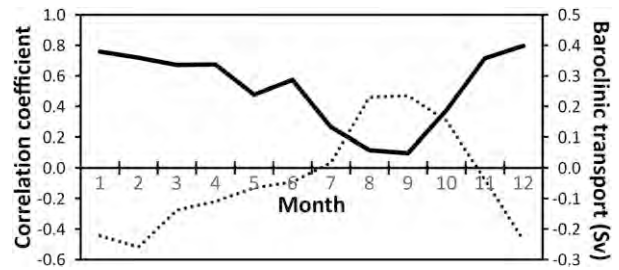


FIG. 9. Monthly variations of correlation of anomalies of sea level difference between Wakkanai and Abashiri vs those of the SWC transport (solid). Superimposed is the baroclinic transport (dotted), which can be a measure of the velocity structure. The positive and negative transports correspond to the surface-intensified and bottom-intensified structures, respectively.

between the ERA-Interim and ERA-40 data, we calculated the regression of the monthly ATW derived from the two datasets for the overlapping period of 1979–2001 and used the ERA-40 ATW regressed into ERA-Interim for the period 1971–78.

Time series of monthly inverted ATW is superimposed in Fig. 7b. The seasonal variation of the inverted ATW averaged over the period of HF radar (2003–15) is also shown in Fig. 6b. The inverted ATW shows seasonal variations similar to those of the SLD and SWC transport, which is consistent with its role on the seasonal variations of the Japan Sea Throughflow (Tsujino et al. 2008; Kida et al. 2016). On the other hand, the seasonal signal is too strong in Fig. 7b, and thus it conceals the interannual variability. To remove the effect of seasonal variations, we calculated the correlation of the inverted ATW with the inverted sea level at Abashiri, SLD, and SWC transport for each month during the 12 yr. The inverted ATW is significantly correlated only in winter months (December, January, and February), with the inverted sea level at Abashiri ( $R = 0.69, 0.85, \text{ and } 0.43$ ) and accordingly with the SLD ( $R = 0.84, 0.90, \text{ and } 0.68$ ) and the SWC transport ( $R = 0.43, 0.72, \text{ and } 0.48$ ), where  $R$  for the 99% significance level is 0.71–0.73. Thus, we show the time series of these for the best correlated month of January for the period 1971–2015 (Fig. 11a). Even for 45 yr, the inverted ATW is well correlated with the inverted sea level at Abashiri ( $R = 0.66$ ) and further with the SLD ( $R = 0.65$ ), where  $R$  for the 99% significance level is 0.38. Figure 11b shows the correlations of the inverted ATW with the inverted sea level at Abashiri and the SLD for each month during 1971–2015, confirming that the ATW is significantly correlated with the sea level and SLD only in the winter seasons. Because the SLD well reflects the SWC transport in winter, as shown in section 4, the ATW can be a key determinant for the interannual variation of the SWC transport as well as for the seasonal variation.

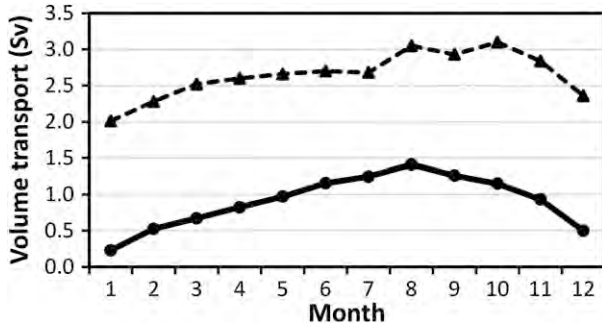


FIG. 10. The seasonal variations of the volume transport of the Tsushima Warm Current (dashed) from the 10-yr average (Fukudome et al. 2010) and of the Soya Warm Current (solid) from the 12-yr average in this study.

Finally, we examine whether interannual variations of the ATW can quantitatively explain those of Abashiri sea level and the SLD [referring, in part, to Nakanowatari and Ohshima (2014)], in which the seasonal variation of the sea level dominated by the ATW is quantified. Assuming that the current variation associated with the ATW is barotropic and horizontally uniform, the amplitude of the geostrophic current speed  $\Delta u$  is represented by

$$\Delta u = (g/f)(\Delta\eta/\Delta x), \quad (5)$$

where  $\Delta x$  is the width of the ATW,  $g$  is the acceleration of gravity ( $9.8 \text{ m s}^{-2}$ ), and  $\Delta\eta$  is the amplitude of the sea level at the coast, where the offshore sea level is assumed to be constant. The variation of the volume transport  $\Delta V$  can be calculated by  $\Delta V = \Delta u \times H \times \Delta x$ , where  $H$  is the mean water depth over the width of the ATW. Using Eq. (5),  $\Delta V$  is represented by

$$\Delta V = (g/f)\Delta\eta H. \quad (6)$$

If we adopt  $H = 100 \text{ m}$ , following Nakanowatari and Ohshima (2014), and  $\Delta\eta = 0.1 \text{ m}$  from Fig. 11a,  $\Delta V$  is estimated to be  $\sim 0.9 \text{ Sv}$ . The interannual variation of the theoretical ATW transport calculated using the wind stress is  $0.5\text{--}1.0 \text{ Sv}$  from Fig. 11a. Hence, the order of the theoretical value is comparable to the value estimated from  $\Delta\eta$ , suggesting that the ATW can explain the sea level variation quantitatively.

## 7. Heat, salt, and dense water transports

Given a vertical section of temperature, salinity, and alongshore velocity of the SWC (Figs. 4, 5), we calculate the heat and salt transports through the Soya Strait. In a

conventional manner, we define the heat transport relative to a temperature of  $0^\circ\text{C}$  as follows:

$$Fh = \iint \rho_w c_w T v dA, \quad (7)$$

where  $c_w$ ,  $T$ ,  $v$ , and  $A$  are the specific heat, temperature, alongshore velocity, and area of a section of the SWC, respectively. We define the salt transport in the following simple way:

$$Fs = \iint \rho_w (S \times 10^{-3}) v dA, \quad (8)$$

where  $S$  is the salinity. This salt transport is converted to the freshwater volume transport  $Fw$ , with the relationship  $Fw = (Fs \times 10^3)/(\rho_w S_0)$ , where  $S_0$  is the reference salinity. Monthly and annual values of the heat and salt transports are listed in Table 1. The annual-mean heat and salt transports are  $25.5 \text{ TW}$  and  $31.15 \times 10^6 \text{ kg s}^{-1}$ , respectively. The heat transport shows the seasonal variations roughly similar to those of the SWC-averaged temperature, while it increases rapidly from July to August, in accordance with a rapid increase of the surface-intensified flow (Fig. 5a) with warmer water.

In the present dataset, the temperature and salinity averaged annually over all the water that comes through the Soya Strait are calculated to be  $6.90^\circ\text{C}$  and  $33.61$ , respectively. The water temperature and salinity averaged over the whole Okhotsk Sea down to the bottom are estimated to be  $1.78^\circ\text{C}$  and  $33.91$ , respectively, based on the dataset of Ohshima et al. (2014). With respect to the averages of all the water masses in the Okhotsk Sea, the heat flux through the Soya Strait is positive, while the salt flux is negative to the averages, with the annual fluxes being  $+19 \text{ TW}$  and  $-0.28 \times 10^6 \text{ kg s}^{-1}$ , respectively. When the calculation is made from the surface to a depth of  $600 \text{ m}$  in the Okhotsk Sea, where the SWC water with a maximum density of  $27.1\sigma_\theta$  can reach, the temperature and salinity averages are  $1.39^\circ\text{C}$  and  $33.38$ , respectively. In terms of the role on the net budget, the SWC salt flux should be regarded as positive.

Watanabe and Wakatsuchi (1998) proposed that the dense water from the Soya Strait in winter and spring can be a potential source of Okhotsk Sea Intermediate Water, which is finally ventilated into the intermediate layer of the North Pacific (Talley 1991). They regarded the inflowing water with a density greater than  $26.8\sigma_\theta$  as the potential source and estimated its annual flux as  $0.20 \text{ (Sv)}$ . We here estimated the volume flux of dense water with  $>26.8\sigma_\theta$  from our dataset (Table 1). The dense water flux occurs from February through August, with a maximum of  $0.50 \text{ Sv}$  in March and April. The

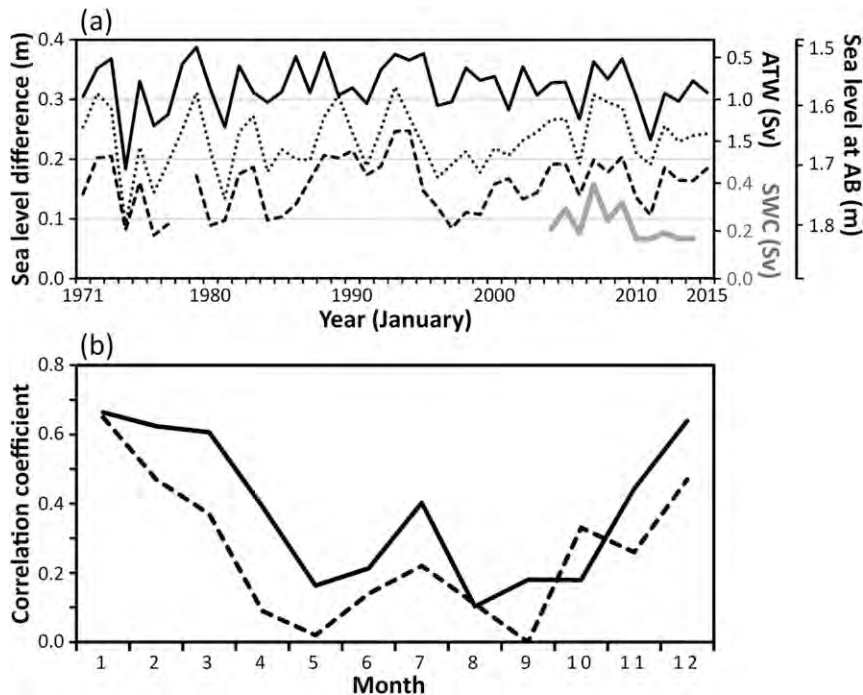


FIG. 11. (a) Time series of the ATW (solid), sea level at Abashiri (dotted), the SLD (dashed), and the SWC transport (thick gray) in January for 45 yr (1971–2015). The scales of the ATW transport and sea level at Abashiri (AB) are indicated on the right axis and inverted. (b) Monthly variations of the correlation of the inverted ATW with inverted sea level at Abashiri (solid) and the SLD (dashed) for 45 yr (1971–2015).

annual-mean flux is 0.18 Sv, which is consistent with Watanabe and Wakatsuchi (1998). The annual-mean flux estimated by Itoh et al. (2003), 0.08 Sv, is less than half the value calculated in the present study. This is because Itoh et al. (2003) underestimated the current speed and excluded the March volume due to missing data.

## 8. Discussion

### a. Heat budget in the Japan Sea

Once the heat flux through the Soya Strait is given, we attempted to evaluate the heat balance in the Japan Sea using only the observational data. The heat balance in the Japan Sea is given by

$$DH = Fh_n + Q_n, \quad (9)$$

where  $DH$ ,  $Fh_n$ , and  $Q_n$  are the temporal changes of the heat content of the Japan Sea, the net horizontal heat flux due to ocean currents through the three straits, and the net surface heat flux averaged over the Japan Sea, respectively. The values of heat flux  $Fh$  and volume transport  $Fv$  through the three straits are represented as follows:

$$Fh_n = Fh_1 - Fh_2 - Fh_3, \quad \text{and} \quad (10)$$

$$Fv_1 = Fv_2 + Fv_3, \quad (11)$$

where the subscripts  $i = 1, 2, 3$  correspond to the Tsushima–Korea, Tsugaru, and Soya Straits, respectively. Hirose et al. (1996) conducted the first quantitative evaluation of the heat balance of the Japan Sea with its seasonal variations. That study assumed that the transports through the three straits are constant throughout the year. In this study, we evaluate the heat balance by considering the seasonal variations of the volume transports. Monthly values of  $Fh_3$  and  $Fv_3$  are provided by this study (Table 1). We used the monthly values of  $Fv_1$  estimated by Fukudome et al. (2010), listed in Table 2. The monthly values of  $Fv_2$  are assumed to be  $Fv_1 - Fv_3$ .

We estimated  $Fh_i$  ( $i = 1, 2$ ) as follows:

$$Fh_i = \rho_w c_w T_i Fv_i, \quad (12)$$

where  $T_i$  is the long-term monthly mean of water temperature at the section of Tsushima–Korea and Tsugaru Straits. The values of  $T_i$  were calculated from all available JODC data files. We took the cross-shore sections perpendicular to the mainstreams at the eastern and

TABLE 2. Monthly and seasonal-mean values of volume transport (Sv), heat flux (TW), and mean water temperature ( $^{\circ}\text{C}$ ) at the three straits. Monthly volume transports through the Tsushima–Korea Strait (column 2) are averages during 1997–2007 estimated by Fukudome et al. (2010). Seasonal volume transports (column 3) and heat flux (column 4) through the Tsushima–Korea Strait are averages during the 1990s estimated by Isobe et al. (2002), where the 3-month means are calculated. The mean water temperatures at the Tsushima–Korea and Tsugaru Strait sections (dotted lines in Fig. 1) are calculated from all the data within the rectangular areas designated in Fig. 1. Analogous values are shown for the Soya Strait; in that case the means are calculated by averaging over the inflow water (Fig. 5b).

Month	Tsushima–Korea			Temperature ( $^{\circ}\text{C}$ )	Tsugaru	Soya
	$Fv_1$ (Fuku) (Sv)	$Fv_1$ (Isobe) (Sv)	$Fh_1$ (Isobe) (TW)		Temperature ( $^{\circ}\text{C}$ )	Temperature ( $^{\circ}\text{C}$ )
1	2.01			15.1	9.6	1.8
2	2.28	1.90	110	14.0	9.0	0.7
3	2.52			13.8	7.8	1.5
4	2.60			14.5	8.2	2.5
5	2.66	2.40	150	16.0	9.8	4.0
6	2.70			17.5	11.7	5.4
7	2.68			18.7	14.5	7.0
8	3.05	2.70	200	20.5	17.8	11.0
9	2.93			21.3	17.9	11.8
10	3.10			20.7	17.3	10.5
11	2.84	2.50	200	19.6	15.4	7.7
12	2.36			17.6	13.4	5.3
Mean	2.64	2.38	165	17.7	12.7	6.9

western channels of the Tsushima–Korea Strait and at the western mouth of the Tsugaru Strait (dotted lines in Fig. 1). All the data within the rectangular areas (designated in Fig. 1) were then projected onto the cross-shore section (dotted line). The cross-shore section dataset was then constructed with an  $e$ -folding scale and influence radius of 5 km. Data that fell outside three standard deviations from the mean at each depth were eliminated. Finally,  $T_i$  were calculated by averaging over the section for each month (Table 2).

Monthly values of  $Fh_n$  calculated from Eq. (10) are presented in Table 3. Regarding  $Fh_1$  and  $Fv_1$ , Isobe et al. (2002) estimated the seasonal (3-month mean) values based on the section observations (Table 2). We also calculated seasonal values of  $Fh_n$  (Table 3) using the results of Isobe et al. (2002). Using the monthly  $Fh_n$  in Table 3, with monthly  $Q_n$  provided by Hirose et al. (1996), we calculated the monthly DH from Eq. (9) and presented them in Fig. 12. When no significant warming or cooling in the Japan Sea is assumed, the annual-mean DH should be zero and the annual-mean  $Fh_n$  and  $Q_n$  are balanced on a long-term time average. The significant, large, positive values of the annual-mean  $Fh_n$ ,  $\sim 60$ – $75$  TW, is roughly consistent with the annual-mean  $Q_n$  estimated in previous studies [e.g., 54 TW by Hirose et al. (1996); 40 TW from the ERA-Interim reanalysis (Dee et al. 2011)]. In contrast to  $Q_n$ ,  $Fh_n$  is positive throughout the year (Fig. 12). The  $Fh_n$  exhibits the maximum value in June, delayed by about a half year from the maximum heat loss in December. This is likely explained by the advection time:

water cooled in winter over the Japan Sea reaches the Soya Strait by about a half year and flows out from the Japan Sea, resulting in the larger positive  $Fh_n$ .

We admit that still there is nonnegligible uncertainty in our estimation, particularly in estimation of heat fluxes at Tsushima–Korea and Tsugaru Straits. We also calculated the velocity-weighted average temperatures at the two straits, assuming that the velocity linearly increases toward the surface in warm seasons (May–November) with the surface velocity being 3 times the velocity at the deepest bin, referring the velocity structure at the Tsushima–Korea Strait (Takikawa et al. 2005) and the Tsugaru Strait (Shikama 1994). The calculated temperatures are higher by  $0.2^{\circ}$ – $0.9^{\circ}\text{C}$ , and the resultant heat budget changes only slightly ( $Fh_n$  is increased by 1.8 TW).

#### b. Heat/salt budgets in the Okhotsk Sea

Next we attempted to evaluate the heat and salt/freshwater budgets in the Okhotsk Sea by using the heat and salt fluxes through the Soya Strait. For these budgets, water exchange with the North Pacific is an important component as well as the fluxes from the Soya Strait. Water exchange between the Okhotsk Sea and the North Pacific occurs through the Kuril Straits, with a net inflow into the Okhotsk Sea at the northern straits and a net outflow through the southern straits, mainly the Bussol' Strait (Moroshkin 1968; Ohshima et al. 2010; Katsumata and Yasuda 2010). Katsumata et al. (2004) estimated the net volume, heat, and salt transports through the Bussol' Strait based on repeated CTD and

TABLE 3. Monthly and annual-mean values of net heat flux via ocean currents  $Fh_n$  through the Tsushima–Korea, Tsugaru, and Soya Straits in the Japan Sea, with net surface heat flux  $Q_n$  from Hirose et al. (1996) and temporal changes of heat content DH. The unit is in TW. Column 3 shows the seasonal mean  $Fh_n$ , calculated from the volume and heat fluxes through the Tsushima–Korea Strait estimated by Isobe et al. (2002).

Month	$Fh_n$	$Fh_n$ (Isobe)	$Q_n$ (Hirose)	DH
1	52.3		−284	−231
2	64.4	56.3	−179	−115
3	79.3		−22	57
4	86.5		80	167
5	90.6	75.9	135	225
6	93.7		134	227
7	84.0		127	211
8	73.1	51.0	84	157
9	72.7		−35	37
10	75.6		−135	−59
11	77.5	67.0	−250	−173
12	57.0		−300	−243
Mean	75.6	62.5	−54	22

lowered ADCP observations across the strait. Although the inflow and outflow between the Okhotsk Sea and North Pacific exhibits large seasonal variations (Ohshima et al. 2010), temperature and salinity profiles do not show large seasonal variations (confirmed by the profiling float observations) due to strong vertical mixing in the straits (Ono et al. 2013). We therefore assumed that the transport estimate of Katsumata et al. (2004) through the Bussol' Strait during August–September is the annual mean and used that value in the transport calculations as a first approximation.

According to Katsumata et al. (2004), of the net outflow of 9.0 Sv, water with a density less than  $27.0\sigma_\theta$  accounts for 5.13 Sv. Because the density of the SWC water is at most  $27.0\sigma_\theta$ , we assume that all the SWC water exits through the Bussol' Strait, that is, of the 5.13 Sv of water with a density less than  $27.0\sigma_\theta$  that flows out, an annual mean of 0.91 Sv is from the SWC water. The corresponding heat and salt fluxes are therefore assumed to be 0.91/5.13 times the fluxes associated with all water with a density less than  $27.0\sigma_\theta$ . The resultant heat outflow is 7.0 TW, and the salt outflow is  $30.96 \times 10^6 \text{ kg s}^{-1}$ . Putting inflow by the SWC and its outflow together, the net heat and salt fluxes become positive values of 19 TW and  $0.19 \times 10^6 \text{ kg s}^{-1}$ , respectively.

We here evaluate the contribution of heat and salt fluxes through the Soya Strait. According to Ohshima et al. (2003) and Nihashi et al. (2012), the estimated annual net surface heat flux is  $-22 \text{ W m}^{-2}$ , averaged over the entire Sea of Okhotsk. This flux corresponds to the total heat loss of 31 TW for the entire Okhotsk

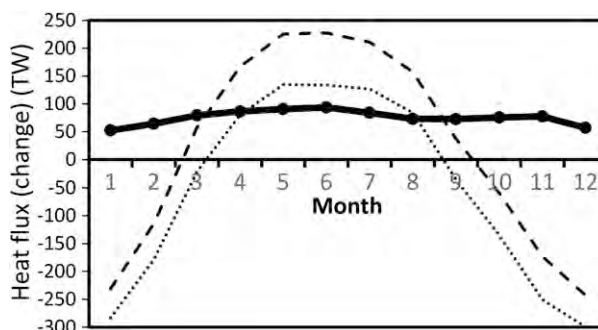


FIG. 12. Seasonal variations of the heat budget in the Japan Sea (TW). Shown are the net heat flux via ocean currents through the three straits ( $Fh_n$ ) (solid), the net surface heat flux averaged over the seas  $Q_n$  from Hirose et al. (1996) (dotted), and the temporal changes of the heat content in the sea DH (dashed).

Sea; that is, the Okhotsk Sea loses heat to the atmosphere. The magnitude of warming by the current system associated with the SWC is the same order but somewhat smaller relative to the atmospheric cooling. The remaining warming is likely made by water exchange with the North Pacific, as suggested by Katsumata et al. (2004).

The net salt flux of  $+0.19 \times 10^6 \text{ kg s}^{-1}$  is converted to the freshwater flux of  $-5.51 \text{ mSv}$  by assuming a salinity of 33.61 as the reference inflow salinity. This is equivalent to a freshening of  $-0.12 \text{ m yr}^{-1}$  averaged over the Okhotsk Sea. According to Dai et al. (2009), the freshwater flux from the Amur River is 9.83 mSv, equivalent to a freshening of  $0.22 \text{ m yr}^{-1}$ . From the ERA-Interim reanalysis (Dee et al. 2011), the excess rate of precipitation over evaporation (P–E) averaged over the Okhotsk Sea is  $0.28 \text{ m yr}^{-1}$ . Salinization from the Soya Strait flux partially balances the Amur River discharge and P–E. Salinization via water exchange with the North Pacific through the Kuril Straits is another important component of the salt balance. These estimates suggest that the contribution of the heat and salt fluxes through the Soya Strait are comparable to the net surface heat flux, the river discharge, and P–E.

## 9. Conclusions

The present study provided climatological values of the mean and seasonal variations of the volume transport through the Soya Strait for the first time. This information has been the missing link of the Japan Sea Throughflow system. The annual-mean volume transport is estimated to be 0.91 Sv, with a maximum (1.41 Sv) in August and a minimum (0.23 Sv) in January (Table 1; Fig. 6a). In the annual mean, the TSC transport is portioned to TGC by 60% and to SWC by 40%. On the other hand, a

major part of the seasonal variation in TSC transport is shared by that in SWC transport (Fig. 10).

This study is consistent in that the SWC is primarily driven by the sea level difference between the Japan Sea and the Sea of Okhotsk. The study suggests that integration of the wind stress along the east coast of Sakhalin and farther upstream [arrested topographic waves (ATW)] determines the sea level difference (SLD). The dominant northerly or northwesterly winds induce a setup of the sea level along the east coast of Sakhalin in winter. This setup propagates to the Hokkaido coast and raises the sea level toward the coast on the Okhotsk side around the Soya Strait. We propose that this setup causes a reduction of the SLD through the Soya Strait and thus decreases the volume transport in winter. This scenario is consistent with the model and analytical work of Tsujino et al. (2008) and Kida et al. (2016). As well as such seasonal variations, interannual variations of the transport in winter are likely determined by the wind stress along the east coast of Sakhalin through the SLD (Fig. 11). In cold seasons (November to April), the monthly volume transport is strongly correlated with the sea level difference (Wakkanai–Abashiri), and we introduced an empirical formula to estimate the transport from the sea level difference [Eq. (3)].

The present study also provides the climatological values of heat and salt/freshwater transports through the Soya Strait. The annual-mean heat and salt transports are 25.5 TW (reference temperature of 0°C) and  $31.15 \times 10^6 \text{ kg s}^{-1}$ , respectively (Table 1). Using these estimates, we can close the heat and salt/freshwater budgets for the Japan Sea and also the Sea of Okhotsk, although the estimate is still rough mainly because of the uncertainty in estimation of heat/salt fluxes at other straits. The annual-mean heat flux via ocean currents through the three straits in the Japan Sea is estimated to be ~60–75 TW. In the Sea of Okhotsk, the net heat flux by the inflow through the Soya Strait and its outflow provides 19 TW, which can be a major contributor to the balance with atmospheric cooling. The net salt flux via the inflow and outflow provides  $0.19 \times 10^6 \text{ kg s}^{-1}$ . The inflow water with a density  $>26.8\sigma_\theta$  through the Soya Strait can be a source of Okhotsk Sea Intermediate Water and further North Pacific Intermediate Water. Its annual-mean flux is estimated to be 0.18 Sv in this study.

*Acknowledgments.* The authors express their gratitude to Yasushi Fukamachi and Masaaki Wakatsuchi for their instructive comments, Toru Takatsuka for his contribution to the operation of the HF radar system, and Kyoko Kitagawa for her support in data processing. Thanks are also extended to the Hokkaido Central and Wakkanai Fisheries Experimental Stations for their cooperation. The tide gauge records and meteorological data used in

the present study were downloaded from the websites of the Japan Oceanographic Data Center (JODC) and Japan Meteorological Agency (JMA), respectively. The JMA GPV data were obtained from the website of the Research Institute for Sustainable Humanosphere, Kyoto University. This work was supported by Grants-in-Aid 17310002, 18201002, and 16H02226 for scientific research from the Ministry of Education, Culture, Sports, Science and Technology of Japan.

## REFERENCES

- Aota, M., 1975: Studies on the Soya Warm Current (in Japanese with English abstract). *Low Temp. Sci.*, **33A**, 151–172.
- , and M. Matsuyama, 1987: Tidal current fluctuations in the Soya Current. *J. Oceanogr. Soc. Japan*, **43**, 276–282, doi:10.1007/BF02108695.
- Barrick, D. E., and B. J. Lipa, 1997: Evolution of bearing determination of HF current mapping radars. *Oceanography*, **10**, 72–75, doi:10.5670/oceanog.1997.27.
- , M. W. Evans, and B. L. Weber, 1977: Ocean surface currents mapped by radar. *Science*, **198**, 138–144, doi:10.1126/science.198.4313.138.
- Csanady, G. T., 1978: The arrested topographic wave. *J. Phys. Oceanogr.*, **8**, 47–62, doi:10.1175/1520-0485(1978)008<0047:TATW>2.0.CO;2.
- Dai, A., T. Qian, and K. E. Trenberth, 2009: Changes in continental freshwater discharge from 1948 to 2004. *J. Climate*, **22**, 2773–2792, doi:10.1175/2008JCLI2592.1.
- Dee, D. P., and Coauthors, 2011: The ERA-Interim reanalysis: Configuration and performance of the data assimilation system. *Quart. J. Roy. Meteor. Soc.*, **137**, 553–597, doi:10.1002/qj.828.
- Ebuchi, N., Y. Fukamachi, K. I. Ohshima, K. Shirasawa, M. Ishikawa, T. Takatsuka, T. Daibo, and M. Wakatsuchi, 2006: Observation of the Soya Warm Current using HF ocean radar. *J. Oceanogr.*, **62**, 47–61, doi:10.1007/s10872-006-0031-0.
- , —, —, and M. Wakatsuchi, 2009: Subinertial and seasonal variations in the Soya Warm Current revealed by HF ocean radars, coastal tide gauges, and bottom-mounted ADCP. *J. Oceanogr.*, **65**, 31–43, doi:10.1007/s10872-009-0003-2.
- Fukamachi, Y., I. Tanaka, K. I. Ohshima, N. Ebuchi, G. Mizuta, H. Yoshida, S. Takayanagi, and M. Wakatsuchi, 2008: Volume transport of the Soya Warm Current revealed by bottom-mounted ADCP and ocean-radar measurement. *J. Oceanogr.*, **64**, 385–392, doi:10.1007/s10872-008-0031-3.
- , K. I. Ohshima, N. Ebuchi, T. Bando, K. Ono, and M. Sano, 2010: Volume transport in the Soya Strait during 2006–2008. *J. Oceanogr.*, **66**, 685–696, doi:10.1007/s10872-010-0056-2.
- Fukudome, K., J.-H. Yoon, A. Ostrovskii, T. Takikawa, and I.-S. Han, 2010: Seasonal volume transport variation in the Tsushima Warm Current through the Tsushima Straits from 10 years of ADCP observations. *J. Oceanogr.*, **66**, 539–551, doi:10.1007/s10872-010-0045-5.
- Hirose, N., C.-H. Kim, and J.-H. Yoon, 1996: Heat budget in the Japan Sea. *J. Oceanogr.*, **52**, 553–574, doi:10.1007/BF02238321.
- Ishizu, M., Y. Kitade, and M. Matsuyama, 2008: Characteristics of the cold-water belt formed off Soya Warm Current. *J. Geophys. Res.*, **113**, C12010, doi:10.1029/2008JC004786.
- Isobe, A., S. Tawara, A. Kaneko, and M. Kawano, 1994: Seasonal variability in the Tsushima Warm Current,

- Tsushima-Korea Strait. *Cont. Shelf Res.*, **14**, 23–35, doi:10.1016/0278-4343(94)90003-5.
- , M. Ando, T. Watanabe, T. Senjyu, S. Sugihara, and A. Manda, 2002: Freshwater and temperature transports through the Tsushima-Korea Straits. *J. Geophys. Res.*, **107** (C7), doi:10.1029/2000JC000702.
- Ito, T., and Coauthors, 2003: Variation of velocity and volume transport of the Tsugaru Warm Current in the winter of 1999–2000. *Geophys. Res. Lett.*, **30**, 1678, doi:10.1029/2003GL017522.
- Itoh, M., and K. I. Ohshima, 2000: Seasonal variations of water masses and sea level in the southwestern part of the Okhotsk Sea. *J. Oceanogr.*, **56**, 643–654, doi:10.1023/A:1011121632160.
- , —, and M. Wakatsuchi, 2003: Distribution and formation of Okhotsk Sea Intermediate Water: An analysis of isopycnal climatological data. *J. Geophys. Res.*, **108**, 3258, doi:10.1029/2002JC001590.
- Jacobs, G. A., H. T. Perkins, W. J. Teague, and P. J. Hogan, 2001: Summer transport through the Tsushima-Korea Straits. *J. Geophys. Res.*, **106**, 6917–6929, doi:10.1029/2000JC000289.
- Katsumata, K., and I. Yasuda, 2010: Estimates of non-tidal exchange transport between the Sea of Okhotsk and the North Pacific. *J. Oceanogr.*, **66**, 489–504, doi:10.1007/s10872-010-0041-9.
- , K. I. Ohshima, T. Kono, M. Itoh, I. Yasuda, Y. N. Volkov, and M. Wakatsuchi, 2004: Water exchange and tidal currents through the Bussol' Strait revealed by direct current measurements. *J. Geophys. Res.*, **109**, C09S06, doi:10.1029/2003JC001864.
- Kida, S., B. Qiu, J. Yang, and X. Lin, 2016: The annual cycle of the Japan Sea Throughflow. *J. Phys. Oceanogr.*, **46**, 23–39, doi:10.1175/JPO-D-15-0075.1.
- Large, W. G., and S. Pond, 1981: Open ocean momentum flux measurements in moderate to strong winds. *J. Phys. Oceanogr.*, **11**, 324–336, doi:10.1175/1520-0485(1981)011<0324:OOMFMI>2.0.CO;2.
- Lyu, S. J., and K. Kim, 2003: Absolute transport from the sea level difference across the Korea Strait. *Geophys. Res. Lett.*, **30**, 1285, doi:10.1029/2002GL016233.
- , and —, 2005: Subinertial to interannual transport variations in the Korea Strait and their possible mechanisms. *J. Geophys. Res.*, **110**, C12016, doi:10.1029/2004JC002651.
- Matsuyama, M., M. Aota, I. Ogasawara, and S. Matsuyama, 1999: Seasonal variation of Soya Current (in Japanese with English abstract). *Umi no Kenkyu*, **8**, 333–338.
- , M. Wadaka, T. Abe, M. Aota, and Y. Koike, 2006: Current structure and volume transport of the Soya Warm Current in summer. *J. Oceanogr.*, **62**, 197–205, doi:10.1007/s10872-006-0044-8.
- Minato, S., and R. Kimura, 1980: Volume transport of the western boundary current penetrating into a marginal sea. *J. Oceanogr. Soc. Japan*, **36**, 185–195, doi:10.1007/BF02070331.
- Mizuta, G., K. I. Ohshima, Y. Fukamachi, M. Itoh, and M. Wakatsuchi, 2004: Winter mixed layer and its yearly variability under sea ice in the southwestern part of the Sea of Okhotsk. *Cont. Shelf Res.*, **24**, 643–657, doi:10.1016/j.csr.2004.01.006.
- , —, —, and M. Wakatsuchi, 2005: The variability of the East Sakhalin Current induced by winds over the continental shelf and slope. *J. Mar. Res.*, **63**, 1017–1039, doi:10.1357/00224005775247625.
- Morimoto, A., A. Watanabe, G. Onitsuka, T. Takikawa, M. Moku, and T. Yanagi, 2012: Interannual variations in material transport through the eastern channel of the Tsushima/Korea Straits. *Prog. Oceanogr.*, **105**, 38–46, doi:10.1016/j.pocean.2012.04.011.
- Moroshkin, K. V., 1968: Water masses of the Sea of Okhotsk. U.S. Department of Commerce Joint Publications Research Service 43942, 196 pp.
- Na, H., Y. Isoda, K. Kim, Y. H. Kim, and S. J. Lyu, 2009: Recent observations in the straits of the East/Japan Sea: A review of hydrography, currents and volume transports. *J. Mar. Syst.*, **78**, 200–205, doi:10.1016/j.jmarsys.2009.02.018.
- Nakanowatari, T., and K. I. Ohshima, 2014: Coherent sea level variation in and around the Sea of Okhotsk. *Prog. Oceanogr.*, **126**, 58–70, doi:10.1016/j.pocean.2014.05.009.
- Nihashi, S., K. I. Ohshima, and N. Kimura, 2012: Creation of a heat and salt flux dataset associated with sea ice production and melting in the Sea of Okhotsk. *J. Climate*, **25**, 2261–2278, doi:10.1175/JCLI-D-11-00022.1.
- Nishida, Y., I. Kanomata, I. Tanaka, S. Sato, S. Takahashi, and H. Matsubara, 2003: Seasonal and interannual variations of the volume transport through the Tsugaru Strait (in Japanese with English abstract). *Umi no Kenkyu*, **12**, 487–499.
- Odamak, M., 1994: Tides and tidal currents along the Okhotsk coast of Hokkaido. *J. Oceanogr.*, **50**, 265–279, doi:10.1007/BF02239517.
- Ohshima, K. I., 1994: The flow system in the Japan Sea caused by a sea level difference through shallow straits. *J. Geophys. Res.*, **99**, 9925–9940, doi:10.1029/94JC00170.
- , and M. Wakatsuchi, 1990: A numerical study of barotropic instability associated with the Soya Warm Current in the Sea of Okhotsk. *J. Phys. Oceanogr.*, **20**, 570–584, doi:10.1175/1520-0485(1990)020<0570:ANSOBI>2.0.CO;2.
- , and D. Simizu, 2008: Particle tracking experiments on a model of the Okhotsk Sea: Toward oil spill simulation. *J. Oceanogr.*, **64**, 103–114, doi:10.1007/s10872-008-0008-2.
- , T. Watanabe, and S. Nihashi, 2003: Surface heat budget of the Sea of Okhotsk during 1987–2001 and the role of sea ice on it. *J. Meteor. Soc. Japan*, **81**, 653–677, doi:10.2151/jmsj.81.653.
- , T. Nakanowatari, S. Riser, and M. Wakatsuchi, 2010: Seasonal variation in the in- and outflow of the Okhotsk Sea with the North Pacific. *Deep-Sea Res. II*, **57**, 1247–1256, doi:10.1016/j.dsr2.2009.12.012.
- , —, —, Y. Volkov, and M. Wakatsuchi, 2014: Freshening and dense shelf water reduction in the Okhotsk Sea linked with sea ice decline. *Prog. Oceanogr.*, **126**, 71–79, doi:10.1016/j.pocean.2014.04.020.
- Ono, K., K. I. Ohshima, T. Kono, K. Katsumata, I. Yasuda, and M. Wakatsuchi, 2013: Distribution of vertical diffusivity in the Bussol' Strait: A mixing hot spot in the North Pacific. *Deep-Sea Res. I*, **79**, 62–73, doi:10.1016/j.dsr.2013.05.010.
- Ostrovskii, A., K. Fukudome, J.-H. Yoon, and T. Takikawa, 2009: Variability of the volume transport through the Korea/Tsushima Strait as inferred from the shipborne acoustic Doppler current profiler observations in 1997–2007. *Oceanology*, **49**, 338–349, doi:10.1134/S0001437009030060.
- Seo, G.-H., Y.-K. Cho, and B.-J. Choi, 2014: Variations of heat transport in the northwestern Pacific marginal seas inferred from high-resolution reanalysis. *Prog. Oceanogr.*, **121**, 98–108, doi:10.1016/j.pocean.2013.10.005.
- Shcherbina, A. Y., L. D. Talley, and D. L. Rudnick, 2003: Direct observations of North Pacific ventilation: Brine rejection in the Okhotsk Sea. *Science*, **302**, 1952–1955, doi:10.1126/science.1088692.
- Shikama, N., 1994: Current measurement in the Tsugaru Strait using the bottom-mounted ADCPs (in Japanese). *Kaiyo Mon.*, **26**, 815–818.

- Simizu, D., and K. I. Ohshima, 2006: A model simulation on the circulation in the Sea of Okhotsk and the East Sakhalin Current. *J. Geophys. Res.*, **111**, C05016, doi:10.1029/2005JC002980.
- Takikawa, T., and J.-H. Yoon, 2005: Volume transport through the Tsushima Straits estimated from sea level difference. *J. Oceanogr.*, **61**, 699–708, doi:10.1007/s10872-005-0077-4.
- , —, and K.-D. Cho, 2005: The Tsushima Warm Current through Tsushima Straits estimated from ferryboat ADCP data. *J. Phys. Oceanogr.*, **35**, 1154–1168, doi:10.1175/JPO2742.1.
- Talley, L. D., 1991: An Okhotsk Sea water anomaly: Implications for ventilation in the North Pacific. *Deep-Sea Res.*, **38A**, S171–S190, doi:10.1016/S0198-0149(12)80009-4.
- Tanaka, I., and A. Nakata, 1999: Results of direct current measurement in the La Perouse Strait (the Soya Strait), 1995–1998. *PICES Sci. Rep.*, **12**, 173–176.
- Teague, W. J., G. A. Jacobs, H. T. Perkins, J. W. Book, K.-I. Chang, and M.-S. Suk, 2002: Low-frequency current observations in the Korea/Tsushima Strait. *J. Phys. Oceanogr.*, **32**, 1621–1641, doi:10.1175/1520-0485(2002)032<1621:LFCOIT>2.0.CO;2.
- , P. A. Hwang, G. A. Jacobs, J. W. Book, and H. T. Perkins, 2005: Transport variability across the Korea/Tsushima Strait and the Tsushima Island wake. *Deep-Sea Res. II*, **52**, 1784–1801, doi:10.1016/j.dsr2.2003.07.021.
- Toba, Y., K. Tomizawa, Y. Kurasawa, and K. Hanawa, 1982: Seasonal and year-to-year variability of the Tsushima-Tsugaru Warm Current system with its possible cause. *Mer*, **20**, 41–51.
- Toulany, B., and C. J. R. Garrett, 1984: Geostrophic control of fluctuating flow through straits. *J. Phys. Oceanogr.*, **14**, 649–655, doi:10.1175/1520-0485(1984)014<0649:GCOFBF>2.0.CO;2.
- Tsujino, H., H. Nakano, and T. Motoi, 2008: Mechanism of currents through the straits of the Japan Sea: Mean state and seasonal variation. *J. Oceanogr.*, **64**, 141–161, doi:10.1007/s10872-008-0011-7.
- Watanabe, T., and M. Wakatsuchi, 1998: Formation of 26.8–26.9  $\sigma_\theta$  water in the Kuril Basin of the Sea of Okhotsk as a possible origin of North Pacific Intermediate Water. *J. Geophys. Res.*, **103**, 2849–2865, doi:10.1029/97JC02914.
- Zhang, W., N. Ebuchi, Y. Fukamachi, and Y. Yoshikawa, 2016: Estimation of wind drift current in the Soya Strait. *J. Oceanogr.*, **72**, 299–311, doi:10.1007/s10872-015-0333-1.